

Vibration control of a stay cable with a rotary electromagnetic inertial mass damper

Zhi Hao Wang^{*1}, Yan Wei Xu¹, Hui Gao¹, Zheng Qing Chen², Kai Xu² and Shun Bo Zhao¹

¹International Joint Research Lab for Eco-building Materials and Engineering of Henan Province, North China University of Water Resources and Electric Power, Zhengzhou 450045, China

²College of Civil Engineering, Hunan University, Changsha 410082, China

(Received October 18, 2016, Revised January 12, 2019, Accepted January 25, 2019)

Abstract. Passive control may not provide enough damping for a stay cable since the control devices are often restricted to a low location level. In order to enhance control performance of conventional passive dampers, a new type of damper integrated with a rotary electromagnetic damper providing variable damping force and a flywheel serving as an inertial mass, called the rotary electromagnetic inertial mass damper (REIMD), is presented for suppressing the cable vibrations in this paper. The mechanical model of the REIMD is theoretically derived according to generation mechanisms of the damping force and the inertial force, and further validated by performance tests. General dynamic characteristics of an idealized taut cable with a REIMD installed close to the cable end are theoretically investigated, and parametric analysis are then conducted to investigate the effects of inertial mass and damping coefficient on vibration control performance. Finally, vibration control tests on a scaled cable model with a REIMD are performed to further verify mitigation performance through the first two modal additional damping ratios of the cable. Both the theoretical and experimental results show that control performance of the cable with the REIMD are much better than those of conventional passive viscous dampers, which mainly attributes to the increment of the damper displacement due to the inertial mass induced negative stiffness effects of the REIMD. Moreover, it is concluded that both inertial mass and damping coefficient of an optimum REIMD will decrease with the increase of the mode order of the cable, and oversize inertial mass may lead to negative effect on the control performance.

Keywords: stay cable; rotary electromagnetic damper; inertial mass; negative stiffness; modal damping ratio

1. Introduction

Long steel cables, commonly used in cable-stayed bridges, are prone to unwanted vibrations due to their small ratio of mass to length and extremely low intrinsic damping. Large vibrations may reduce the cable service life and seriously affect safe operation of cable-stayed bridges. Several effective countermeasures have been presented and/or implemented to mitigate such vibrations, and especially transverse dampers are often installed near the anchorage of the cable. Discrete passive viscous dampers attached perpendicularly to cables have been successfully used in a number of bridges. However, lots of studies have demonstrated that control performance of a cable with a passive damper is greatly restricted by the small ratio between damper location and cable length in practical situations (Kovacs 1982, Pacheco *et al.* 1993, Krenk 2000, Main and Jones 2002, Wang *et al.* 2005, Fujino and Hoang 2008, Cheng *et al.* 2010, Zhou *et al.* 2014). For longer bridge cables, such as the Sutong Bridge and the Stonecutters Bridge with a main span of 1088 m and 1018 m, respectively, the induced additional modal damping ratio of a passive damper may not be enough to suppress the

problematic vibration of a cable without significantly detracting the aesthetics of the bridge.

To solve this problem, two dampers attached on a single cable (Caracoglia and Jones 2007) and hybrid control with both crossies and dampers (Zhou *et al.* 2015, Ahmad *et al.* 2018, He *et al.* 2018) are proposed. However, these systems may be complicated and costly. As an alternative, semi-active control has been also presented to improve control performance since they offer the capability of active control devices without the requirement of large power resources (Johnson *et al.* 2003). In particular, MR dampers have attracted extensive attention from the community because of their excellent performance in both lab tests and engineering practice (Spencer *et al.* 1997, Ni *et al.* 2002, Chen *et al.* 2004, Chistenson *et al.* 2006, Duan *et al.* 2005, Duan *et al.* 2006, Cai *et al.* 2007, Liu *et al.* 2007, Li *et al.* 2007, Or *et al.* 2008, Weber *et al.* 2011, Huang *et al.* 2012, Weber *et al.* 2015, Duan *et al.* 2018). To date, it has been applied to cable vibration control systems on the Dongting Lake Bridge (Chen *et al.* 2004), Binzhou Bridge (Li *et al.* 2007) and Sutong Bridge (Weber and Distl 2015a). However, these systems still require external and stable power supply, which may be impossible or unassured in some extreme events, such as earthquakes and typhoons. To avoid external power supply, self-powered MR damper (Choi and Wereley 2006, Jung *et al.* 2008, Sapiński 2008, Wang *et al.* 2018) based on vibration energy harvesting by electromagnetic induction technology have been proposed,

*Corresponding author, Associate Professor
E-mail: wangzhihao@ncwu.edu.cn

and its excellent control performance has been experimentally confirmed by Kim *et al.* (2010).

Excellent control performance of stay cables with semi-active MR dampers can be attributed to negative stiffness characteristics (Li *et al.* 2008), which has also been found in the vibration control area of seismically excited bridges (Pradono *et al.* 2009). The role of such negative stiffness has been well demonstrated (Høgsberg 2011, Weber and Distl 2015b). The results show that the introduction of negative stiffness yields an apparent local softening the structure at damper position (Høgsberg 2011), and makes damper move with larger displacement (Iemura and Pradono 2003, Li *et al.* 2008), thus dissipating more energy. In view of this, some efforts have also been attempted to enhance control performance of stay cables with viscous dampers by introducing the negative stiffness device based on pre-compressed spring (Chen *et al.* 2015, Zhou and Li 2016), which concluded that such control system can effectively increase modal damping ratios of the cable. Similar findings were also reported by Shi *et al.* (2016).

Another source of negative stiffness is the inerter, which was originally proposed by Smith *et al.* (2002). In the area of civil engineering, the inerter was called apparent mass (Ikago *et al.* 2012) or inertial mass (Garrido *et al.* 2013, Nakamura *et al.* 2014). Until recently, control performance of viscous inertial mass damper or tuned inerter damper to mitigate cables vibration have been investigated and proved (Lazar *et al.* 2016, Lu *et al.* 2017, Shi and Zhu 2018, Luo *et al.* 2019). However, viscous fluid inside viscous dampers may leak over time, which is the main concern of this kind of dampers. As a non-contacted damping strategy, eddy current damping (Sodano and Bae 2004) and electromagnetic damping (Palomera *et al.* 2008, Zhu *et al.* 2012, Zhu *et al.* 2019) are two possible alternative solutions for this problem. Control performance of stay cables with passive electromagnetic dampers was also experimentally validated (Shen *et al.* 2016). To further confirm the superior control performance of inertial mass dampers, a rotary electromagnetic inertial mass damper (REIMD) for suppressing cable vibrations is constructed and investigated via both theoretical analysis and experimental investigations in this paper. The proposed REIMD consists of a rotary electromagnetic damper (RED) for energy dissipation, a ball screw that translates linear motion of the cable into high-speed rotational motion of the RED, and a flywheel attached to the shaft of the RED as the inertial mass element.

This paper first gives the mechanical model of the REIMD via both theoretical analysis and experimental validation, and then the dynamic characteristics of a taut cable with a REIMD installed close to the cable end is theoretically investigated, where the effects of inertial mass and damping coefficient on modal damping ratios of the cable are highlighted. Finally, control performance of a model cable with a REIMD are experimentally evaluated by the identified modal damping ratios in the first two modes of the cable and corresponding control mechanics of the REIMD are subsequently discussed and obtained.

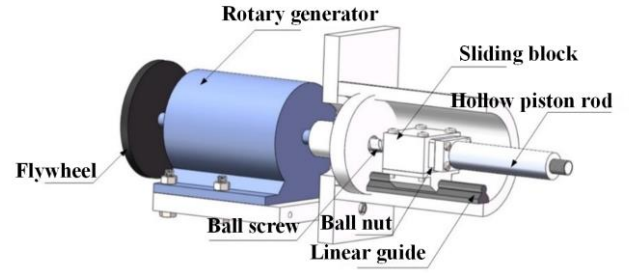


Fig. 1 Schematic diagram of a REIMD

2. Configuration and mechanical model of the REIMD

2.1 Configuration of the REIMD

The proposed REIMD, depicted in Fig. 1, mainly consists of a rotary generator, a ball screw, a liner guide way and a flywheel. The linear motion of the hollow piston rod connected to the main structure can be converted into the high-speed rotational motion of the rotary generator and the flywheel through ball screw amplification mechanism, where the liner guide way is set in the REIMD with the function of ensuring the REIMD move smoothly. The inertial forces generated by the mass moment of inertia of the flywheel and the generator itself are again amplified when they are translated back to the axial direction of the REIMD.

2.2 Mechanical model of the REIMD

According to the configuration of the REIMD shown in Fig. 1, the total axial force of the REIMD consists of three parts, such as the damping force provided by the rotary generator, the inertial force generated by the flywheel and the generator, and the friction force generated between the brush and armature as well as the ball screw mechanism. Therefore, the total axial force of the REIMD can be expressed as

$$f(t) = F_d + F_i + F_f = c_{eq} \frac{du}{dt} + m_e \frac{d^2u}{dt^2} + f_0 \text{sign}(\dot{u}) \quad (1)$$

where F_c , F_i and F_f denote the damping force, the inertial force, and the friction force, respectively; u and \dot{u} denote the axial displacement and the axial velocity of the REIMD; c_{eq} , m_e and f_0 denote the equivalent damping coefficient, the inertial mass and the friction force of the REIMD, respectively; $\text{sign}(\dot{u})$ is the signum function that gives 1, 0 or -1 according to the sign condition of \dot{u} .

If the self-inductance effect can be negligible, the equivalent damping coefficient c_{eq} of the REIMD can be expressed as (Palomera *et al.* 2008, Zhu *et al.* 2012)

$$c_{eq} = \frac{(k_e \eta)^2}{R_a + R_l} \quad (2)$$

where k_e denotes the electromotive force constant, R_a and R_L denote the internal resistance and the load resistance of the generator, respectively, η denotes the transformation coefficient of linear motion to the rotational motion through the ball screw mechanism with the expression as

$$\eta = \frac{2\pi}{L_d} \quad (3)$$

The inertial mass m_e of the REIMD can be expressed as (Nakamura *et al.* 2014)

$$m_e = \eta^2(I_f + I_g) \quad (4)$$

where I_f and I_g denote the moment of inertia of the flywheel and the generator, respectively.

When the sinusoidal excitation $u = u_0 \sin(\omega t)$ is applied to the REIMD, the axial force of the REIMD in Eq. (1) can be rewritten as

$$f(t) = -m_e \omega^2 u + c_{eq} \dot{u} + f_0 \text{sign}(\dot{u}) \quad (5)$$

Eq. (5) clearly indicates that the REIMD can produce negative stiffness effects, and corresponding negative stiffness can be described as

$$k = -m_e \omega^2 \quad (6)$$

2.3 Experimental validation

Mechanical performance tests of the REIMD with design parameters in Table 1 are conducted to verify the established mechanical model of the REIMD. A CFX-04 speed-measuring permanent magnet motor shown in Fig. 2 is employed as the rotary generator of the REIMD. The mechanical performance test setup of the REIMD is shown in Fig. 3. The REIMD is forced to rotate synchronously with a servo motor, where the loading frequency and amplitude of the excitation system can be adjusted by the frequency transformer and the eccentricity of the eccentric wheel, respectively.

Table 1 Design parameters of the REIMD

Generator	Internal resistance	R_a	6.4Ω
	Electromotive force constant	k_e	0.06V/(r·min ⁻¹)
	Maximum angular velocity	n	3000r/min
	Moment of inertia	I_g	8.00 kg·cm ²
Ball screw	Diameter	D	16 mm
	Lead	L_d	16 mm
Flywheel	Moment of inertia (small)	I_{f-s}	5.05 kg·cm ²
	Moment of inertia (medium)	I_{f-m}	11.28 kg·cm ²
	Moment of inertia (large)	I_{f-L}	22.00 kg·cm ²



Fig. 2 A rotary electromagnetic damper



Fig. 3 Mechanical performance test setup of the REIMD

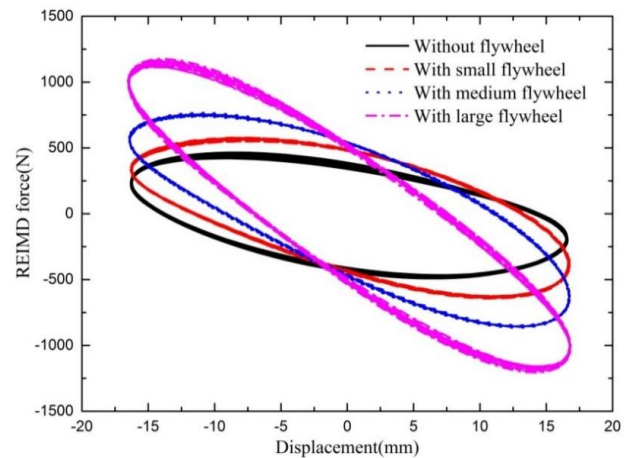


Fig. 4 The force-displacement hysteresis loops of the REIMD with different flywheel (load resistance: 50Ω)

A load cell and a displacement gauge are used to measure the axial force and displacement of the REIMD, respectively. The loading frequency is 2 Hz, and loading displacement amplitude is 17 mm.

Fig. 4 shows the force-displacement relationship of the REIMD with different flywheel. It can be seen that both the slope of the hysteretic loops and corresponding negative stiffness of the REIMD continuously increase with the increase of the flywheel size. Fig. 5 compares the force time

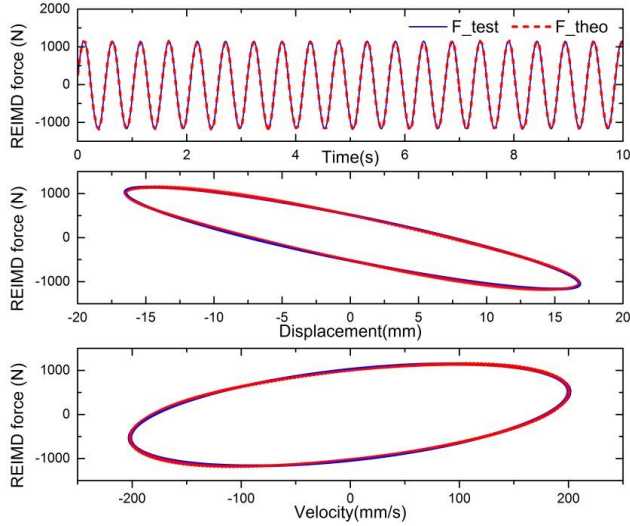


Fig. 5 REIMD force comparisons between theoretical predictions and test results (large flywheel) (Theoretical curves by Eq. (1), $m_e=462.64$ kg, $c_{eq}=2570$ N*s/m, $f_0=0$ N)

histories of theoretical predictions and test results of the REIMD, and the good agreement of each other verifies that the established mechanical model can well describe the mechanical performance of the REIMD.

3. Theoretical analysis of a stay cable with a REIMD

3.1 Dynamic formulation of a stay cable with a REIMD

The schematic diagram of a stay cable with a REIMD is shown in Fig. 6. Neglecting the static deflection, the bending stiffness, the inclination and the inherent damping of the cable, the cable with the length l and the tension T can be idealized as a taut cable with both ends fixed, where a REIMD is perpendicularly installed at the cable in the transverse direction, as shown in Fig. 7.

The transverse free vibrations of a taut cable subjected to a transverse force can be described by the following differential equation (Krenk 2000)

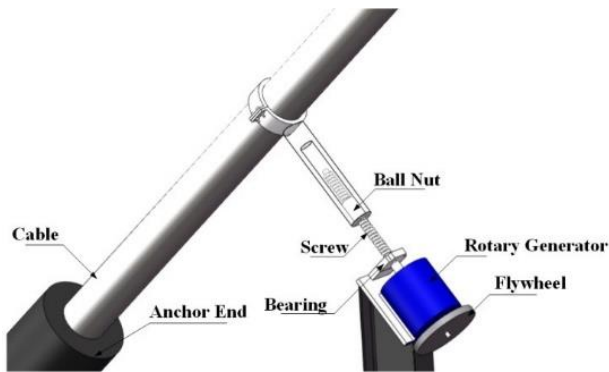


Fig. 6 Schematic diagram of stay cable vibration control with a REIMD

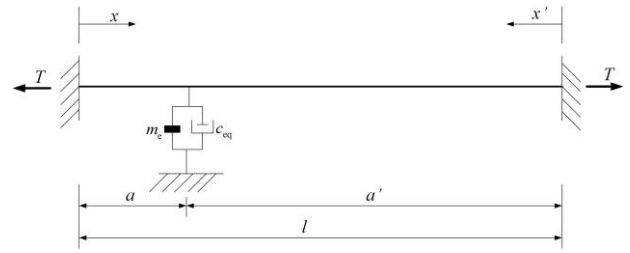


Fig. 7 Schematic representation of a taut cable with a REIMD at $x=a$

$$T \frac{\partial^2 u}{\partial x^2} - m \frac{\partial^2 u}{\partial t^2} = f(t) \delta(x-a) \quad (7)$$

with the boundary condition

$$u(0,t) = u(l,t) = 0 \quad (8)$$

where x is the location coordinate along the cable chord axis, x' is the complementary coordinate defined as $x' = l - x$, $u(x, t)$ is the transverse displacement of the cable at the location x and the time t , m is the cable mass per unit length, $f(t)$ represents the transverse force of the REIMD in Eq. (1), $\delta(\cdot)$ is the Dirac delta function, a is the distance from the cable left end to the REIMD location, and the distance from the cable right end to the REIMD location is calculated as $a' = l - a$.

The concentrated force $f(t)$ causes a discontinuity in $\partial u / \partial x$ at the location $x=a$

$$T \left(\frac{\partial u}{\partial x} \Big|_{a^+} - \frac{\partial u}{\partial x} \Big|_{a^-} \right) = f(t) \quad (9)$$

The transverse displacement of free damped vibrations of the cable can be expressed as

$$u(x,t) = \text{Re}[U(x) \exp(i\omega t)] \quad (10)$$

where ω is the complex natural frequency and $U(x)$ is the complex mode shape of the cable. By substituting Eq. (10) into Eq. (7), the complex mode shape $U(x)$ should satisfy the following ordinary differential equation

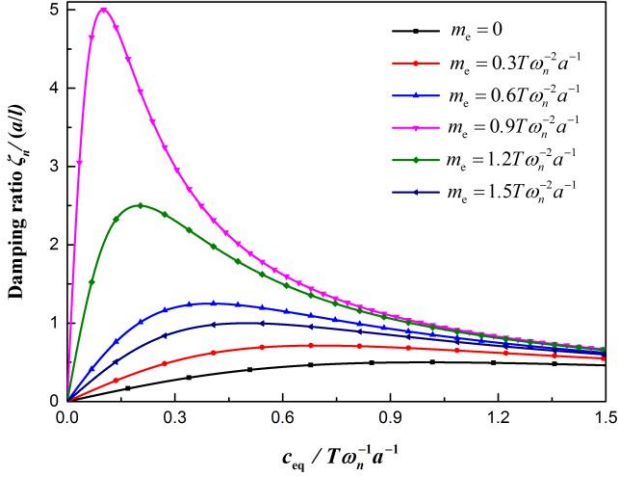
$$\frac{d^2 U}{dx^2} + \beta^2 U = 0 \begin{cases} 0 < x < a \\ 0 < x' < a' \end{cases} \quad (11)$$

where the wave number β has been defined as

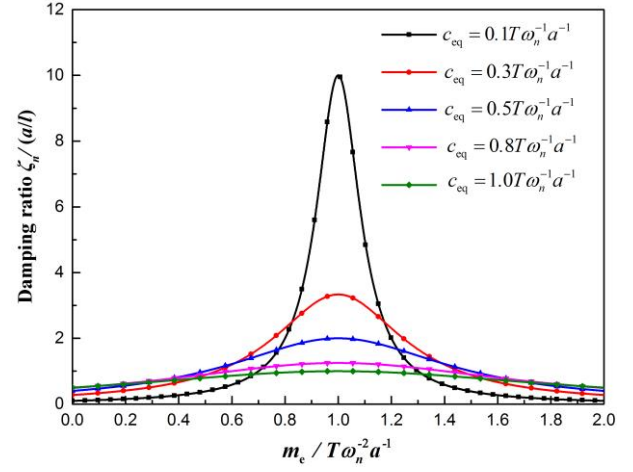
$$\beta = \omega \sqrt{\frac{m}{T}} \quad (12)$$

The solution to Eq. (11) is derived as

$$U(x) = \begin{cases} U_a \frac{\sin(\beta x)}{\sin(\beta a)} & , 0 \leq x \leq a \\ U_a \frac{\sin(\beta x')}{\sin(\beta a')} & , 0 \leq x' \leq a' \end{cases} \quad (13)$$



(a) Variation of modal damping ratio of the cable with damping coefficient of the REIMD



(b) Variation of modal damping ratio of the cable with inertial mass of the REIMD

Fig. 8 The variation of the n^{th} modal damping ratio of the cable with damping coefficient and initial mass of the REIMD

where U_a is the amplitude of the displacement mode shape at the REIMD location. Substitution of the mode shape representation Eq. (13) into the force equilibrium condition Eq. (9) at the REIMD location, the complex wave number β can be determined by

$$\cot(\beta a) + \cot(\beta a') = -\frac{-m_e \omega^2 + c_{\text{eq}} i \omega}{\beta T} \quad (14)$$

It can be further rearranged as

$$\tan(\beta l) = \frac{\sin^2(\beta a)(-m_e \omega^2 + c_{\text{eq}} i \omega)}{\beta T + \sin(\beta a) \cos(\beta a)(-m_e \omega^2 + c_{\text{eq}} i \omega)} \quad (15)$$

As the REIMD is installed close to the cable end ($a \ll l$), the asymptotic solution can be obtained by considering small perturbation of the undamped solution. The wave number corresponding to the n^{th} mode of the undamped cable can be expressed as

$$\beta_n^0 = \frac{n\pi}{l}, n=1,2,\dots \quad (16)$$

Assuming the wave number in the n^{th} mode β_n of the damped cable to be small perturbations from β_n^0 and $a \ll l$, we can achieve the following approximations

$$\tan(\beta_n L) \approx \Delta\beta_n l, \sin(\beta_n a) \approx \beta_n^0 a, \cos(\beta_n a) \approx 1 \quad (17)$$

where $\Delta\beta_n = \beta_n - \beta_n^0$ represents the change of wave number due to the damper force.

Substituting Eq. (17) into Eq. (15) yields

$$\Delta\beta_n = \frac{\beta_n^0 a(-m_e \omega^2 + c_{\text{eq}} i \omega) a}{T + a(-m_e \omega^2 + c_{\text{eq}} i \omega) l} \quad (18)$$

Given the n^{th} mode solution of the wave number β_n , the n^{th} eigen frequency ω_n can be calculated by Eq. (12). The n^{th} eigen frequency relates to the modal damping ratio is

expressed as

$$\omega_n = |\omega_n|(\sqrt{1 - \zeta_n^2} + i\zeta_n) \quad (19)$$

where ζ_n is the n^{th} modal damping ratio and can be solved by

$$\zeta_n = \frac{\text{Im}(\omega_n)}{|\omega_n|} = \frac{\text{Im}(\beta_n)}{|\beta_n|} \approx \frac{\text{Im}(\Delta\beta_n)}{|\beta_n^0|} \quad (20)$$

Substituting Eq. (18) into Eq. (20), the asymptotic solution of n^{th} modal damping ratio of the cable can be finally derived as

$$\zeta_n = \frac{\text{Im}(\omega_n)}{|\omega_n|} = \frac{\text{Im}(\beta_n)}{|\beta_n|} \approx \frac{\text{Im}(\Delta\beta_n)}{|\beta_n^0|} \quad (21)$$

3.2 Optimal damping ratio of the cable and corresponding optimum design of the REIMD

In order to conveniently determine the optimal damping ratio of the cable and the optimum design of the REIMD, the following parameters are defined as

$$\bar{k}_n = -m_e \omega_n^2 a / T, \bar{a} = a / (1 + \bar{k}_n), \eta = \omega_n c_{\text{eq}} \bar{a} / T \quad (22)$$

where \bar{k}_n represents the dimensionless negative stiffness in the n^{th} mode induced by the inertial mass, \bar{a} represents the modified location due to the dimensionless negative stiffness, and η_n denotes the dimensionless damping coefficient in the n^{th} mode. The n^{th} modal damping ratio of the cable can be subsequently derived as

$$\zeta_n = \frac{c_{\text{eq}} \omega_n T a}{(T - m_e \omega_n^2 a)^2 + (c_{\text{eq}} \omega_n a)^2} \frac{a}{l} = \frac{\eta}{1 + \eta^2} \frac{\bar{a}}{l} \quad (23)$$

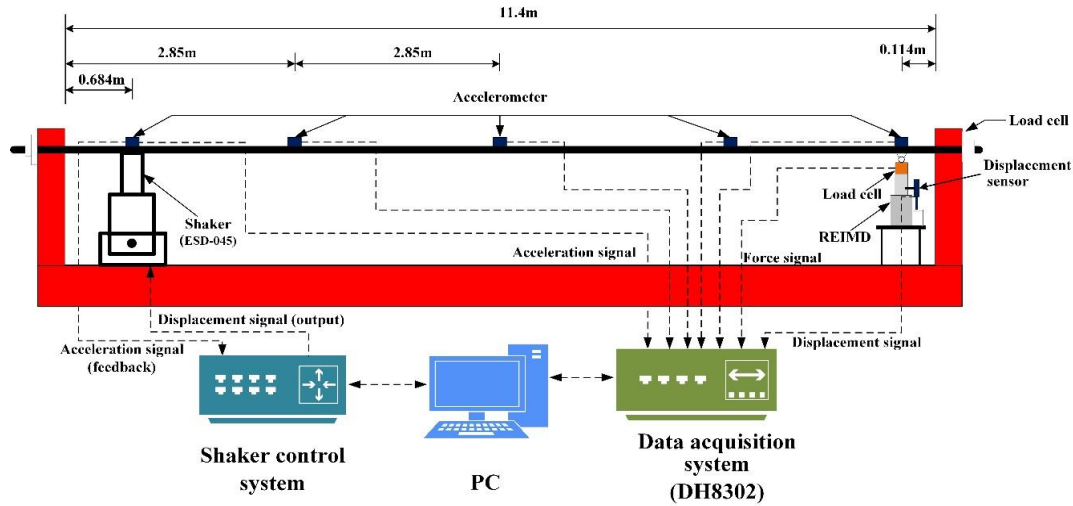


Fig. 9 Schematic diagram of test setup for cable vibration control

Eqs. (22) and (23) indicate that negative stiffness effect of the REIMD is essentially equivalent to installing the traditional viscous damper at relatively higher location. Hence, modal damping ratios of the cable can be significantly enhanced.

The optimum damping coefficient $c_{eq,n}^{opt}$ corresponding to a constant m_e can be obtained by

$$\frac{\partial \zeta_n}{\partial c_{eq}} = 0 \quad (24)$$

Leading the value

$$c_{eq,n}^{opt} = \frac{T}{\omega_n |\bar{a}|} \quad (25)$$

The corresponding optimal damping ratio in the cable n^{th} mode can be obtained as

$$\zeta_n^{opt} = \frac{1}{2} |\bar{a}| / l \quad (26)$$

Eqs. (25) and (26) indicate that both the maximum attainable modal damping ratio of the cable and optimum damping coefficient of the REIMD are related to the modified location of the REIMD, while optimum damping coefficient also relates to the properties of the cable.

Fig. 8 shows the variation of the n^{th} modal damping ratio of the cable with damping coefficient and initial mass of the REIMD. It can be seen that the maximum attainable modal damping of each mode of the cable is the same, while corresponding optimum damping coefficient and initial mass is relatively smaller for a higher mode of the cable.

4. Experiment investigation on vibration control of a stay cable with a REIMD

4.1 Test setup

To further verify vibration control performance of a stay cable with the REIMD, a stay cable model with a REIMD is established in the laboratory. The main properties of the stay cable are shown in Table 2. Fig. 9 illustrates schematic diagram of test setup for cable vibration control, while corresponding photos are shown in Fig. 10. The cable shown in Fig. 10(a) is 11.4 m long with 79 lumped masses attaching on the cable evenly so that the cable model has similar dynamic characteristics with those on real cable-stayed bridges. The REIMD shown in Fig. 10(b), incorporating a load cell and a displacement sensor, is attached transversely to the cable at a location 0.114 m (i.e., 1% of the cable length) from one anchorage, and an electromagnetic shaker shown in Fig. 10(d) is installed at a location 0.684 m (i.e., 6% of the cable length) away from the other anchorage. Accelerator meters are installed at both quarter-span and mid-span of the cable to monitor the cable accelerations, which are adopted to identify the modal damping ratios of the cable. For the measurements, a data acquisition system shown in Fig. 10(c) is employed to collect all the data with 200 Hz sampling frequency, including the forces and the displacements of the REIMD, as well as the acceleration responses of the cable.

Table 2 The main properties of the stay cable

Item	Value
Cable length (l)	11.4 m
Cross-section area (A)	1.374 cm ²
Mass per unit length (m)	9.5 kg/m
Elasticity modulus (E)	200 GPa
Tension force (T)	19.2 kN
Inclination angle (θ)	0°
Sag parameter(λ^2)	4.513
The first modal natural frequency	2.25 Hz
The second modal natural frequency	3.95 Hz

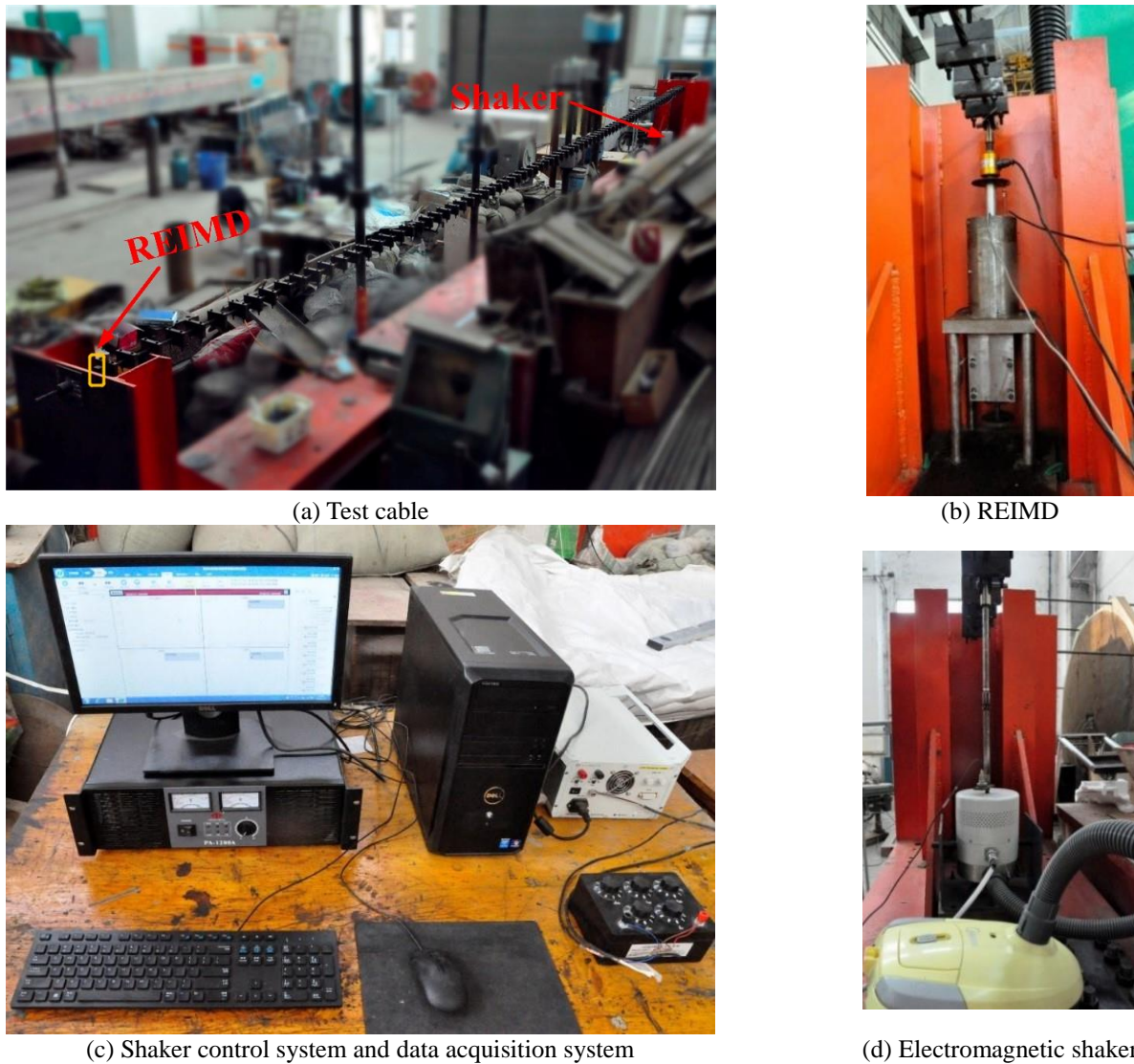


Fig. 10 Test photos for cable vibration control

4.2 Test cases

Series of free vibration tests of the cable are conducted to evaluate the vibration mitigation performance of the REIMD. Test cases for the first two modes of the cable model are summarized in Table 3. Due to the fact that the fundamental frequency of the cable model is too low to be well excited by an electromagnetic shaker, the first mode of the cable is excited by man-power at its natural frequency, while the second mode of the cable is excited by the electromagnetic shaker shown as Fig. 10(d). There are totally six test cases for each of the first two modes of the cable. As for case 1, it is actually a RED without any supplemental inertial mass. The equivalent damping coefficients of the REIMD are adjusted by the load resistance ranging from 0 to 150 Ω . Thus, the effects of the initial mass and the damping coefficient on the control performance of the cable with the REIMD can be derived by the identified modal damping ratios. To identify the modal damping ratio, an exponential function is utilized to

fit the envelope curve of free decay acceleration responses of the cable. Since modal damping ratios may be dependent on the amplitudes of the cable vibrations, the interval accelerations of 4-8 m/s^2 and 6-10 m/s^2 , respectively, are selected to identify the first and the second modal damping ratios of the cable for each case.

4.3 First mode test results

Fig. 11 shows typical time history responses of accelerations at mid-span of the cable for the first mode. It is evident that the case 5 shows a faster response reduction compared with the case 1 and without control, which implies that the REIMD can provide larger modal damping ratios. As shown in Fig. 11, the first modal damping ratio of the cable is 0.22% without control, increases to 0.45% for the RED (case 1), and further increases to 1.23% for the REIMD (case 5).

Table 3 Vibration control test cases of the cable model for the first and second mode

case	Parameters of the flywheel			Parameters of the generator		Parameters of the REIMD	
	Diameter d_f (cm)	Thickness t_f (cm)	Moment of inertia I_f (kg·cm ²)	Load resistance R_L (Ω)	Moment of inertia I_g (kg·cm ²)	Load resistance R_L (Ω)	Inertial mass m_e (kg)
1				0-150	8.00	0-150	123.37
2	9	1	5.05	0-150	8.00	0-150	201.25
3	11	1	11.28	0-150	8.00	0-150	297.32
4	13	1	22.00	0-150	8.00	0-150	462.64
5	15.5	1	44.46	0-150	8.00	0-150	809.00
6	19	1	100.38	0-150	8.00	0-150	1671.36

Note: d_f and t_f denote the diameter and thickness of the REIMD flywheel

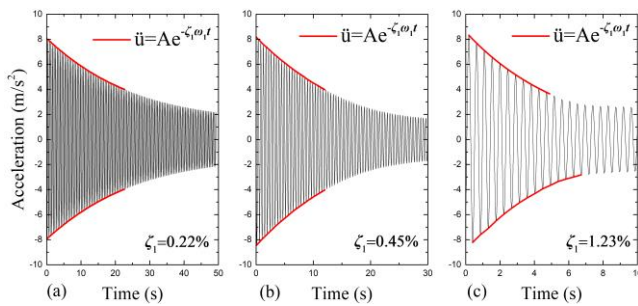


Fig. 11 Time history responses of accelerations at mid-span of the cable for the first mode (a) Without control; (b) RED (case 1) with 40 Ω ; (c) REIMD (case 5) with 40 Ω

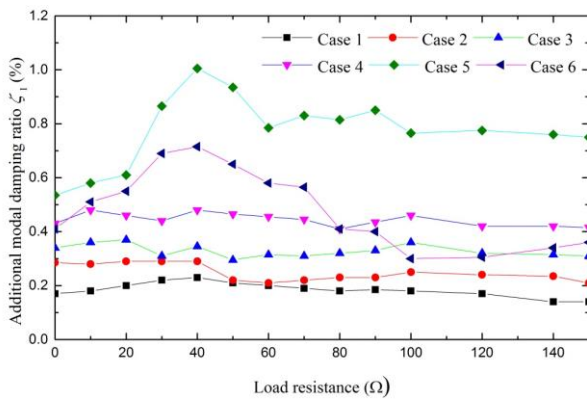


Fig. 12 Plot of additional modal damping ratios versus load resistances for the first mode of the cable

Fig. 12 compares the first modal additional damping ratios of the cable for various control cases. As expected, the attainable maximum first modal additional damping ratios of the cable in the case 2-6 are all larger than those in the case 1. The largest first modal additional optimal damping ratio of the cable is 1.01% when load resistance is 40 Ω for the case 5, while the maximum theoretical optimum damping ratio for a traditional viscous damper is associated with a ratio about half of the ratio between damper location and cable length (Kovacs 1982, Pacheco *et al.* 1993, Krenk 2000, Main and Jones 2002), which is about 0.50% in this paper. The results demonstrate that the largest first modal additional optimal damping ratio of the cable with the REIMD is approximately two times of that

for an optimum viscous damper. However, the first modal additional damping ratios in the case 6 are smaller than those in the case 5, which implies that control performance will be deteriorated when the inertial mass of the REIMD is larger than the optimal value.

4.4 Second mode test results

Harmonic excitation with amplitude 12 mm and 3.95 Hz is adopted to excite the second mode of the cable. The entire process of the acceleration responses of the cable at the quarter-span for the second mode is shown in Fig. 13. It is shown that both the acceleration amplitude and the acceleration root-mean-square (RMS) value of the cable in the case 3 are the smallest among three cases, which demonstrates that the REIMD can also enhance control performance of the cable in the second mode. In addition, as seen from Fig. 14, the second modal damping ratio of the cable is 0.20% without control, increases to 0.98% for the RED (case 1), and further increases to 2.10% for the REIMD (case 4).

Besides, the second modal additional damping ratios of the cable for various control cases are further compared, as shown in Fig. 15. Similar with the first mode of the cable, the attainable maximum second modal additional damping ratios of the cable in the case 2-4 are all larger than those in the case 1. However, the additional damping ratios in the case 5 get smaller than those in the case 1, which implies that the effect of the inertial mass on the control performance of the cable is not always positive. The largest second modal additional damping ratio of the cable can reach 2.23% (load resistance 70 Ω for the case 3), which is 4.46 times of that for an optimum passive viscous damper.

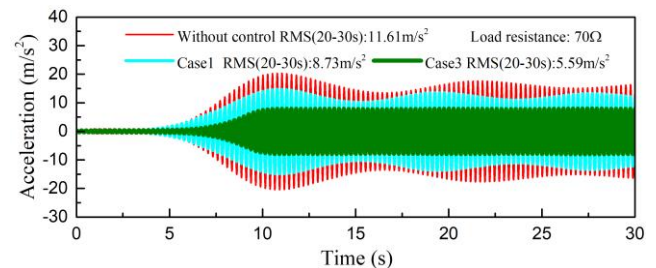


Fig. 13 Forced vibration acceleration responses of the cable at quarter-span for the second mode

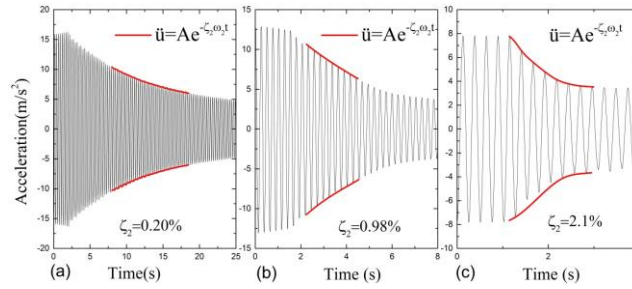


Fig. 14 Time history responses of acceleration at quarter-span of the cable for the second mode (a) Without control; (b) RED (case 1) with 70 Ω and (c) REIMD (case 4) with 70 Ω

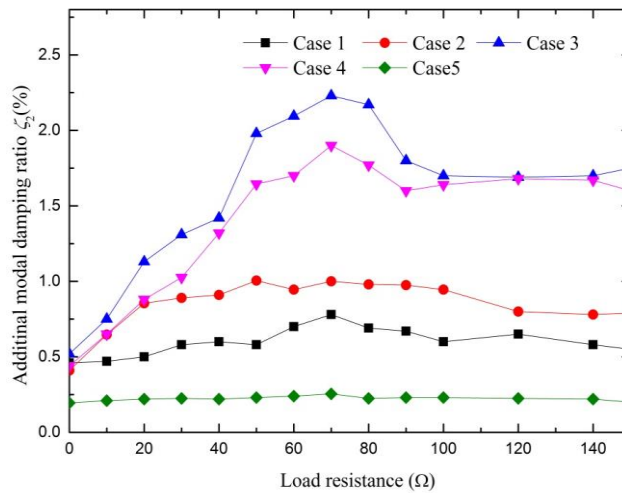


Fig. 15 Plot of additional modal damping ratios versus load resistances for the second mode of the cable

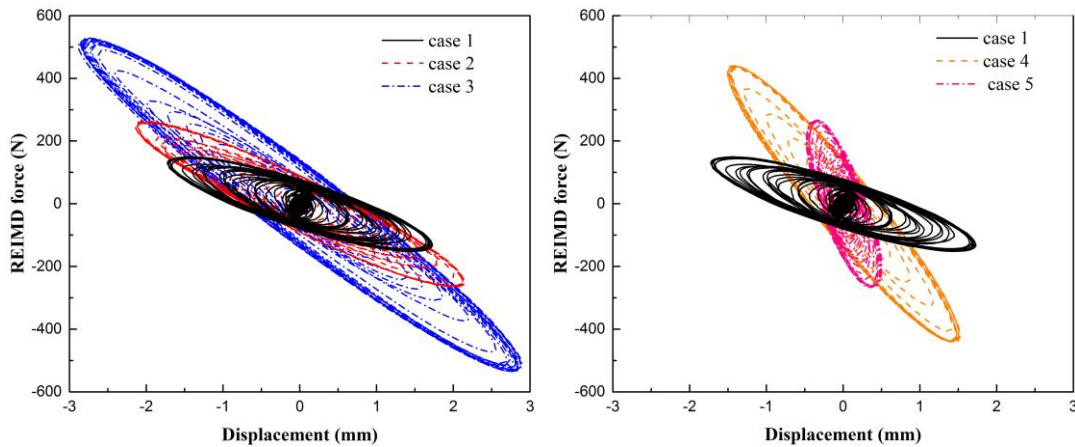


Fig. 16 Hysteretic loops of the REIMD with optimal resistance ($R_L = 70\Omega$, the second mode of the cable)

It is seen that the optimal resistance of the second mode is larger than that of the first mode, and the optimal inertial mass of the second mode (case 3) is smaller than that of the first mode (case 5). Hence, it can be concluded that both the optimal damping coefficient and the inertial mass of the REIMD decrease with the increase of the mode order of the cable, which is consistent with the theoretical analysis results in the section 3.2.

To demonstrate negative stiffness characteristics of the REIMD, Fig. 16 compares typical measured hysteretic loops of the REIMD for the second mode of the cable. Since the load resistance of the REIMD for each case is fixed as 70Ω , corresponding equivalent damping coefficient is almost the same. The REIMD can dissipate more energy with the increase of the damper displacement induced by the inertial mass. However, the displacement of the REIMD will begin to reduce when the inertial mass is beyond

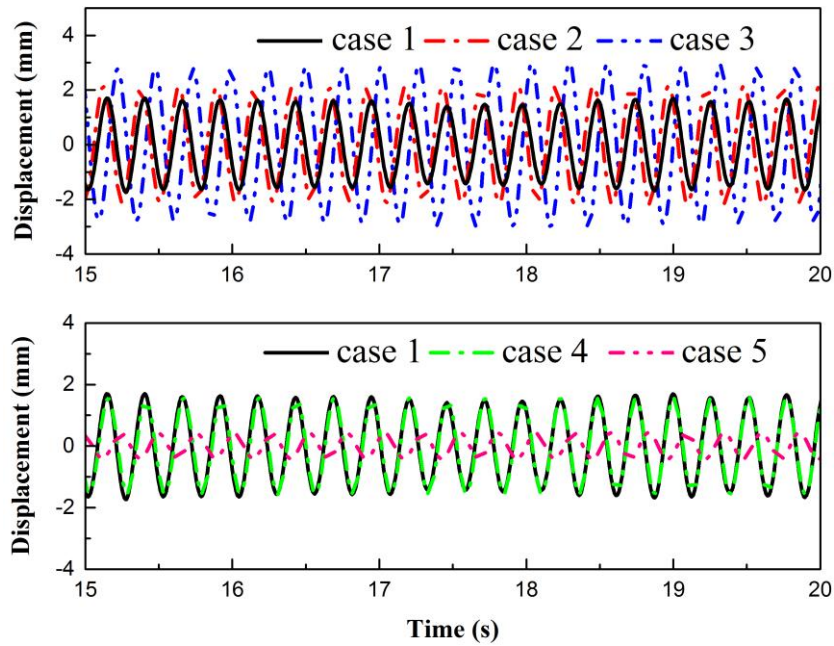


Fig. 17 Displacement time histories of the REIMD with optimal load resistance ($R_L = 70\Omega$, the second mode of the cable)

optimal value depicted as the case 3. Similar comparison results for the displacements of the REIMD are shown in Fig. 17. Hence, there is an optimum inertial mass such that the displacement of the REIMD is most profitably enlarged and the energy dissipation of the REIMD reaches its best efficacy.

4.5 Comparisons of theoretical and test modal damping ratios

Fig. 18 compares theoretically estimated and experimentally identified additional modal damping ratios of the test cable for each test case when the REIMD is with an optimal load resistance. It is seen that the theoretically predicted modal damping ratios are always larger than those test results when the inertial mass of the REIMD is smaller than its optimum value. However, when the inertial mass of REIMD is larger than its optimum value, the theoretically predicted modal damping ratios are always smaller than those test results. There are four main reasons causing the difference between the theoretical and experimental modal damping ratios. (1) The effects of the cable sag (Xu and Yu 1998, Johnson *et al.* 2003, Christenson *et al.* 2006, Duan *et al.* 2019b, Wang *et al.* 2019) has not been evaluated in the ideal taut-cable model adopted in the theoretical analysis. (2) The cable flexural rigidity together with the cable boundary conditions will significantly affect the achievable modal damping ratios of the cable (Fujino and Hoang 2008, Cheng *et al.* 2010), especially for the REIMD has a large negative stiffness (Shi *et al.* 2017). (3) The inevitable support stiffness of the REIMD can also induce the difference between the theoretical and experimental modal damping ratios (Fujino and Hoang 2008, Fournier and Cheng 2014, Duan *et al.* 2019a). (4) There are experimental identification errors of the inertial mass and the equivalent damping coefficient of the REIMD.

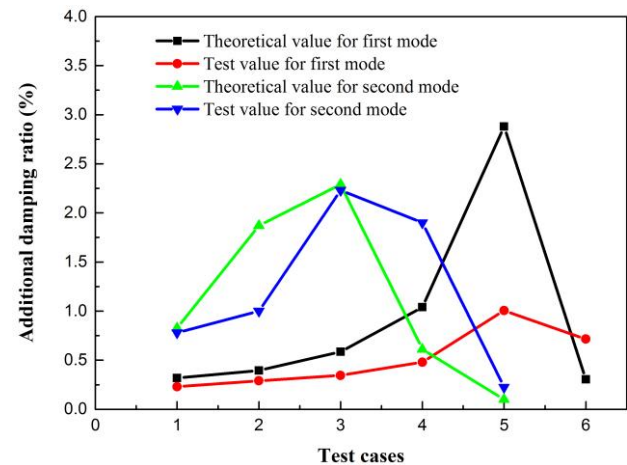


Fig. 18 Comparisons of theoretical and test modal damping ratios of the cable

5. Conclusions

The proposed REIMD can provide variable damping force by a rotary generator with different load resistance and large inertial force with amplified inertial mass through the ball screw mechanism. The accuracy of the derived theoretical mechanical model of the REIMD has been well verified by performance tests. Vibration control of a stay cable with a REIMD was investigated through both theoretical analysis and experimental evaluation. The main conclusions are summarized as follows:

- The theoretical analyses indicate that modal damping ratios of the cable with certain properties are a function of the damping coefficient, the inertial mass and the location of the REIMD. Both the optimum damping coefficient and the inertial mass of the REIMD will decrease with the

increase of mode order of the cable and the location of the REIMD, and increases with the increase of the tension force of the cable.

- The experimental results show that REIMD can provide larger additional modal damping ratios to the cable for the first two modes than those of conventional passive viscous dampers. As for the cable model in this study, the first and second attainable maximum additional modal damping ratios of the cable provided by the REIMD can reach as 2.02 and 4.46 times of the theoretical optimum damping ratios for a passive linear viscous damper, respectively.
- Both the theoretical and experimental results demonstrate that the proposed REIMD can provide superior vibration mitigation performance with respect to conventional passive viscous dampers, and the REIMD is confirmed to be quite feasible and cost-effective for vibration control of stay cables. The excellent control performance of the REIMD mainly owes to negative stiffness effect generated by the inertial mass, which can make the damper move with larger displacements and enhance energy dissipation ability. However, oversize inertial mass of the REIMD may lead to negative effect on the control performance of the cable.

Acknowledgments

The authors greatly acknowledge the financial support from the National Natural Science Foundation of China (Grant No. 51878274 and 51308214) and National Basic Research Program of China (973 Program) (Grant No. 2015CB057702).

References

- Ahmad, J., Cheng, S.H. and Ghrib, F. (2018), "Combined effect of external damper and cross-tie on the modal response of hybrid two-cable networks", *J. Sound. Vib.*, **417**, 132-148. <https://doi.org/10.1016/j.jsv.2017.12.023>.
- Cai, C.S., Wu, W.J. and Araujo, M. (2007), "Cable vibration control with a TMD-MR damper system: experimental exploration", *J. Struct. Eng. - ASCE*, **133**(5), 629-637. [https://doi.org/10.1061/\(ASCE\)0733-9445\(2007\)133:5\(629\)](https://doi.org/10.1061/(ASCE)0733-9445(2007)133:5(629)).
- Caracoglia, L. and Jones, N.P. (2007), "Damping of taut-cable systems, two dampers on a single stay", *J. Eng. Mech. - ASCE*, **133**(10), 1050-1060. [https://doi.org/10.1061/\(ASCE\)0733-9399\(2007\)133:10\(1050\)](https://doi.org/10.1061/(ASCE)0733-9399(2007)133:10(1050)).
- Chen, L., Sun L.M. and Nagarajaiah, S. (2015), "Cable with discrete negative stiffness device and viscous damper: passive realization and general characteristics", *Smart Struct. Syst.*, **15**(3), 627-643. <http://dx.doi.org/10.12989/sss.2015.15.3.627>.
- Smith, M.C. (2002), "Synthesis of mechanical networks: the inerter", *IEEE T. Automat. Contr.*, **47**(10), 1648-1662. <http://dx.doi.org/10.1109/TAC.2002.803532>.
- Chen, Z.Q., Wang, X.Y., Ko, J.M., Ni, Y.Q., Spencer, B.F., Jr., Yang, G. and Hu, J.H. (2004), "MR damping system for mitigating wind-rain induced vibration on Dongting Lake Cable-Stayed Bridge", *Wind Struct.*, **7**(5), 293-304. <http://dx.doi.org/10.1117/12.498072>.
- Cheng, S.H., Darivandi, N. and Ghrib, F. (2010), "The design of an optimal viscous damper for a bridge stay cable using energy-based approach", *J. Sound. Vib.*, **329**(22), 4689-4704. <https://doi.org/10.1016/j.jsv.2010.05.027>.
- Jung, H.J., Jang, J.E., Choi, K.M. and Lee, H.J. (2008), "MR fluid damper-based smart damping systems for long steel stay cable under wind load", *Smart. Struct. Syst.*, **4**(5), 697-710. <https://doi.org/10.12989/sss.2008.4.5.697>.
- Choi, Y.T. and Wereley, N.M. (2006), "Self-powered magneto-rheological dampers", *J. Vib. Acoust.*, **131**(4), 044501(1-5). <https://doi.org/10.1115/1.3142882>.
- Christenson, R.E., Spencer, B.F. and Johnson, E.A. (2006), "Experimental verification of smart cable damping", *J. Eng. Mech. - ASCE*, **132**(3), 268-278. [https://doi.org/10.1061/\(ASCE\)0733-9399\(2006\)132:3\(268\)](https://doi.org/10.1061/(ASCE)0733-9399(2006)132:3(268)).
- Duan, Y.F., Ni, Y.Q. and Ko, J.M. (2005), "State-derivative feedback control of cable vibration using semi-active MR damper", *Comput. - Aided Civ. Inf.*, **20**(6), 431-449. <https://doi.org/10.1111/j.1467-8667.2005.00396.x>.
- Duan, Y.F., Ni, Y.Q. and Ko, J.M. (2006), "Cable vibration control using magneto-rheological (MR) dampers", *J. Intel. Mat. Syst. Str.*, **17**(4), 321-325. https://doi.org/10.1142/9789812702197_0121.
- Duan, Y.F., Tao, J.J., Zhang, H.M., et al. (2018), "Real-time hybrid simulation based on vector form intrinsic finite element and field programmable gate array", *Struct. Control Health Monit.*, **26**(1), e2277. <https://doi.org/10.1002/stc.2277>.
- Duan, Y.F., Ni, Y.Q., Zhang, H.M., et al. (2019a), "Design formulas for vibration control of taut cables using passive MR dampers", *Smart Struct. Syst.*, **23**(6), (in press).
- Duan, Y.F., Ni, Y.Q., Zhang, H.M., et al. (2019b), "Design formulas for vibration control of sagged cables using passive MR dampers", *Smart Struct. Syst.*, **23**(6), (in press).
- Fujino, Y. and Hoang, N. (2008), "Design formulas for damping of a stay cable with a damper", *J. Struct. Eng. - ASCE*, **134**(2), 269-278. [https://doi.org/10.1061/\(ASCE\)07339445\(2008\)134:2\(269\)](https://doi.org/10.1061/(ASCE)07339445(2008)134:2(269)).
- Fournier, J.A. and Cheng, S.H. (2014), "Impact of damper stiffness and damper support stiffness on the efficiency of a linear viscous damper in controlling stay cable vibrations", *J. Bridge Eng. - ASCE*, **19**(4), 04013022. [https://doi.org/10.1061/\(ASCE\)BE.1943-5592.0000562](https://doi.org/10.1061/(ASCE)BE.1943-5592.0000562).
- Garrido, H., Curadelli, O. and Ambrosini, D. (2013), "Improvement of tuned mass damper by using rotational inertial through tuned viscous mass damper", *Eng. Struct.*, **56**(6), 2149-2153. <https://doi.org/10.1016/j.engstruct.2013.08.044>.
- He, X.H., Cai, C., Wang, Z.J., Jimg, H.Q. and Qin, C.W. (2018), "Experimental verification of the effectiveness of elastic cross-ties in suppressing wake-induced vibrations of staggered stay cables", *Eng. Struct.*, **167**, 151-165. <https://doi.org/10.1016/j.engstruct.2018.04.033>.
- Høgsberg, J. (2011), "The role of negative stiffness in semi-active control of magneto-rheological dampers", *Struct. Control Health Monit.*, **18**(3), 289-304. <https://doi.org/10.1002/stc.371>.
- Huang, H., Sun, L.M. and Jiang, X. (2012), "Vibration mitigation of stay cable using optimally tuned MR damper", *Smart Struct. Syst.*, **9**(1), 35-53. <https://doi.org/10.12989/sss.2012.9.1.035>.
- Iemura, H. and Pradono, M.H. (2003), "Application of pseudo negative stiffness control to the benchmark cable-stayed bridges", *Struct. Control Health Monit.*, **10**(3-4), 187-203. <https://doi.org/10.1002/stc.25>.
- Ikago, K., Saito, K. and Inoue, N. (2012), "Seismic control of single-degree-of-freedom structure using tuned viscous mass damper", *Earthq. Eng. Struct. D.*, **41**(3), 453-474. <https://doi.org/10.1002/eqe.1138>.
- Johnson, E.A., Christenson, R.E. and Spencer, B.F. (2003), "Semi-active damping of cables with sag", *Comput. - Aided Civ. Inf.*, **18**(2), 132-146. <https://doi.org/10.1111/1467-8667.00305>.
- Kim, I.H., Jung, H.J. and Koo, J.H. (2010), "Experimental

- evaluation of a self-powered smart damping system in reducing vibration of a full-scale stay cable”, *Smart Mater. Struct.*, **19**(11), 115027(1-10). <https://doi.org/10.1088/0964-1726/19/11/115027>.
- Kovacs, I. (1982), “Zur frage der seil-schwingungen und der seildampfung”, *Bautechnik*, **59**(10), 325-332.
- Krenk, S. (2000), “Vibration of a taut cable with an external damper”, *J. Appl. Mech. - T ASME*, **67**, 772-776. <https://doi.org/10.1115/1.1322037>.
- Lazar, I.F, Neild, S.A. and Wagg, D.J. (2016) “Vibration suppression of cables using tuned inerter dampers”, *Eng. Struct.*, **122**, 62-71. <https://doi.org/10.1016/j.engstruct.2016.04.017>
- Li, H., Liu, M. and Ou, J.P. (2008), “Negative stiffness characteristics of active and semi-active control systems for stay cables”, *Struct. Control Health Monit.*, **15**(2), 120-142. <https://doi.org/10.1002/stc.200>
- Li, H., Liu, M., Li, J.H., Guan, X.C. and Ou, J.P. (2007), “Vibration control of stay cables of Shandong Binzhou Yellow River Highway Bridge by using magnetorheological fluid dampers”, *J. Bridge Eng. -ASCE*, **12**(4), 401-409. [https://doi.org/10.1061/\(ASCE\)1084-0702\(2007\)12:4\(401\)](https://doi.org/10.1061/(ASCE)1084-0702(2007)12:4(401)).
- Liu, M., Song, G.B. and Li, H. (2007), “Non-model-based semi-active vibration suppression of stay cables using magnetorheological fluid damper”, *Smart. Mater. Struct.*, **16**(4), 1447-1452. <https://doi.org/10.1088/0964-1726/16/4/059>.
- Lu, L., Duan, Y.F., Spencer, B.F., Jr., Lu, X. and Zhou, Y. (2017). “Inertial mass damper for mitigating cable vibration”, *Struct. Control Health Monit.*, **24**(10), 1-12. <https://doi.org/10.1002/stc.1986>.
- Luo, J.N., Jiang, J.Z. and Macdonald J.H.G. (2019), “Cable vibration suppression with inerter-based absorbers”, *J. Eng. Mech.*, **145**(2), 04018134. [https://doi.org/10.1061/\(ASCE\)EM.1943-7889.0001554](https://doi.org/10.1061/(ASCE)EM.1943-7889.0001554).
- Main, J.A. and Jones, N.P. (2002), “Free vibration of taut cable with attached damper, I: linear viscous damper”, *J. Eng. Mech. - ASCE*, **128**(10), 1062-1071. [https://doi.org/10.1061/\(ASCE\)0733-9399\(2002\)128:10\(1062\)](https://doi.org/10.1061/(ASCE)0733-9399(2002)128:10(1062)).
- Nakamura, Y., Fukukita, A., Tamura, K., Yamazaki, I., Matsuoka, T. and Sunakoda, K. (2014), “Seismic response control using electromagnetic inertial mass damper”, *Earthq. Eng. Struct. D.*, **43**(4), 507-527. <https://doi.org/10.1002/eqe.2355>.
- Ni, Y.Q., Chen, Y., Ko, J.M. and Cao, D.Q. (2002), “Neuro-control of cable vibration using semi-active magnetorheological dampers”, *Eng. Struct.*, **24**(3), 295-307. [https://doi.org/10.1016/S0141-0296\(01\)00096-7](https://doi.org/10.1016/S0141-0296(01)00096-7).
- Or, S.W., Duan, Y.F., Ni Y.Q., Chen, Z.H. and Lam, K.H. (2008), “Development of magnetorheological dampers with embedded piezoelectric force sensors for structural vibration control”, *J. Intel. Mat. Syst. Str.*, **19**(11), 1327-1338. https://doi.org/10.1142/9789812771209_0047.
- Pacheco, B.M., Fujino, Y. and Sulekh, A. (1993), “Estimation curve for modal damping in stay cables with viscous damper”, *J. Struct. Eng. - ASCE*, **119**, 1961-1979. [https://doi.org/10.1061/\(ASCE\)0733-9445\(1993\)119:6\(1961\)](https://doi.org/10.1061/(ASCE)0733-9445(1993)119:6(1961)).
- Palomera-Arias, R., Connor, J.J. and Ochsendorf, J.A. (2008), “Feasibility study of passiveelectromagnetic damping systems”, *J. Struct. Eng.-ASCE*, **134**, 164-170. [https://doi.org/10.1061/\(ASCE\)0733-9445\(2008\)134:1\(164\)](https://doi.org/10.1061/(ASCE)0733-9445(2008)134:1(164))
- Pradono, M.H., Iemura, H. Igarashi, A., Toyooka, A. and Kalantari, A. (2009), “Passively controlled MR damper in the benchmark structural control problem for seismically excited highway bridge”, *Struct. Control Health Monit.*, **16**(6), 626-638. <https://doi.org/10.1002/stc.341>.
- Sapiński, B. (2008), “An experimental electromagnetic induction device for a magnetorheological damper”, *J. Theor. App. Mech. -POL*, **46**(4), 933-947.
- Shen, W.A., Zhu, S.Y. and Zhu, H.P. (2016), “Experimental study on using electromagnetic devices on bridge stay cables for simultaneous energy harvesting and vibration damping”, *Smart Mater. Struct.*, **25**(6), 065011, 17. <https://doi.org/10.1088/0964-1726/25/6/065011>.
- Shi, X., Zhu, S.Y., Li, J.Y. and Spencer, B.F., Jr. (2016), “Dynamic behavior of stay cables with passive negative stiffness dampers”, *Smart. Mater. Struct.*, **25**(7), 075044. <https://doi.org/10.1088/0964-1726/25/7/075044>
- Shi, X., Zhu, S.Y. and Spencer, B.F. (2017), “Experimental study on passive negative stiffness damper for cable vibration mitigation”, *J. Eng. Mech. - ASCE*, **143**(9), 04017070. [https://doi.org/10.1061/\(ASCE\)EM.1943-7889.0001289](https://doi.org/10.1061/(ASCE)EM.1943-7889.0001289).
- Shi, X. and Zhu S.Y. (2018), “Dynamic characteristics of stay cables with inerter dampers”, *J. Sound Vib.*, **423**, 287-305. <https://doi.org/10.1016/j.jsv.2018.02.042>.
- Sodano, H.A. and Bae, J.S. (2004), “Eddy current damping in structures”, *Shock Vib. Digest*, **36**(6), 469-478. <https://doi.org/10.1177/0583102404048517>.
- Spencer, B.F., Dyke, S.J., Sain, M.K., et al (1997), “Phenomenological model of a magnetorheological damper”, *J. Eng. Mech. - ASCE*, **123**(3), 230-238. <https://doi.org/10.4271/2006-01-2520>.
- Wang, X.Y., Ni, Y.Q., Ko, J.M., et al. (2005), “Optimal design of viscous dampers for multi-mode vibration control of bridge cables”, *Eng.Struct.*, **27**(5), 792-800. <https://doi.org/10.1016/j.engstruct.2004.12.013>.
- Wang, Z.H., Chen, Z.Q., Gao, H., et al. (2018), “Development of a self-powered magnetorheological damper system for cable vibration control”, *Appl. Sci.*, **8**, 1-17. <https://doi.org/10.3390/app8010118>.
- Wang, Z.H., Gao, H., Fan, B.Q. and Chen, Z.Q. (2019), “Inertial mass damper for vibration control of cable with sag”, *J. Low Freq. Noise V. A.*, 1-12.
- Weber, F. and Boston, C. (2011), “Clipped viscous damping with negative stiffness for semi-active cable damping”, *Smart. Mater. Struct.*, **20**(4), 045007. <https://doi.org/10.1088/0964-1726/20/4/045007>.
- Weber, F. and Distl, H. (2015a) “Amplitude and frequency independent cable damping of Sutong Bridge and Russky Bridge by magnetorheological dampers”, *Struct. Control Health Monit.*, **22** (2), 237-254. <https://doi.org/10.1002/stc.1671>.
- Weber, F. and Distl, H. (2015b), “Semi-active damping with negative stiffness for multi-mode cable vibration mitigation: Approximate collocated control solution”, *Smart Mater. Struct.*, **24**(11), 115015. <https://doi.org/10.1088/0964-1726/24/11/115015>.
- Xu, Y. L. and Yu, Z. (1998), “Vibration of inclined sag cables with oil dampers in cable stayed bridges”, *J. Bridge Eng.*, **3**(4), 194-203. [https://doi.org/10.1061/\(ASCE\)1084-0702\(1998\)3:4\(194\)](https://doi.org/10.1061/(ASCE)1084-0702(1998)3:4(194)).
- Zhu, H.P., Li, Y.M., Shen, W.A. and Zhu, S.Y. (2019), “Mechanical and energy-harvesting model for electromagnetic inertial mass dampers”, *Mech. Syst. Signal. Pr.*, **120**, 203-220. <https://doi.org/10.1016/j.ymssp.2018.10.023>.
- Zhu, S.Y., Shen, W.A., Xu, Y.L. and Lee, W.C. (2012), “Linear electromagnetic devices for vibration damping and energy harvesting: Modeling and testing”, *Eng. Struct.*, **34**, 198-212. <https://doi.org/10.1016/j.engstruct.2011.09.024>.
- Zhou, P. and Li, H. (2016), “Modeling and control performance of a negative stiffness damper for suppressing stay cable vibrations”, *Struct. Control Health Monit.*, **23**(4), 764-782. <https://doi.org/10.1002/stc.1809>.
- Zhou, H.J., Sun, L. and Xing, F. (2014), “Damping of full-scale stay cable with viscous damper: Experimentand analysis”, *Adv. Struct. Eng.*, **17**(2), 265-274. <https://doi.org/10.1260/1369-4332.17.2.265>.
- Zhou, H. J., Yang X., Sun, L.M., et al. (2015), “Free vibrations of a two-cable network with near-support dampers and a cross-link”, *Struct. Control Health Monit.*, **22**(9), 1173-1192.

<https://doi.org/10.1002/stc.1738>.